Oriented and Area-Selective Growth of Zeolitic Imidazolate Framework-8 Films by Molecular Layer Deposition

Jorid Smets,[a,b,c] Víctor Rubio-Giménez,[a,†] Jesús Gándara-Loe,[a] Jonas Adriaenssens,[a] Mario Fratschko,[d] Fabian Gasser,[d] Roland Resel,[d] Anita Brady-Boyd,[b, §] Rajeshreddy Ninakanti,[c,e] Steven De Feyter,[f] Silvia Armini,[b] Rob Ameloot[a,]*

[a] Center for Membrane Separations, Adsorption, Catalysis, and Spectroscopy (cMACS), KU Leuven – University of Leuven, Celestijnenlaan 200F, 3001 Leuven, Belgium

[b] Imec, Kapeldreef 75, 3001 Leuven, Belgium

[c] Antwerp Engineering, Photoelectrochemistry and Sensing (A-PECS), Department of Bioscience Engineering, University of Antwerp, Groenenborgerlaan 171, 2020 Antwerp, Belgium

[d] Institute of Solid State Physics, Graz University of Technology, Petersgasse 16, 8010 Graz, Austria

[e] Electron Microscopy for Material Science (EMAT) and NANOlab Center of Excellence, Department of Physics, University of Antwerp, Groenenborgerlaan 171, 2020 Antwerp, Belgium

[f] Department of Chemistry, Division of Molecular Imaging and Photonics, KU Leuven, Leuven, 3001, Belgium

Abstract

Integrating metal-organic frameworks (MOFs) into microfabrication processes will benefit from controlled vapor-phase deposition techniques. This study presents a molecular layer deposition (MLD) method that enables area-selective and oriented growth of zeolitic imidazolate framework 8 (ZIF-8) films. Substrates functionalized with self-assembled monolayers (SAMs) with different end groups (alkyl, phenyl, hydroxyl, carboxyl, amine, and imidazole) allow tuning the degree of crystallographic orientation in the resulting MOF layers. Spatial control over SAM formation determined the surface mobility of the ZIF-8 building blocks, which enabled area-selective deposition.

Controlled deposition is key for integrating thin films of metal-organic frameworks (MOFs) in electronic devices such as sensors and microprocessors.[1–4] However, current solution-based methods are ill-suited due to corrosion, contamination, and surface tension issues.[3] These obstacles can be avoided by developing vapor-phase deposition methods such as chemical vapor deposition (CVD) and molecular layer deposition (MLD).[2,3,5] For instance, these approaches have been successfully demonstrated for a few MOF materials, including ZIF-8.[6–9]

In addition, since MOFs are crystalline materials, some film properties can depend on the crystallographic orientation. Such anisotropy has been demonstrated in optical applications, separations, and conductivity measurements.[10–13] Oriented MOF films have been achieved through various strategies. For example, MOF crystallites with well-developed facets can be assembled on a surface or aligned through magnetic or electric fields.[14–16] When the MOF material is formed on the substrate, specific surface interactions or a dominant growth direction can result in crystallographic orientation.[11] Examples of the former approach include (hetero)epitaxial growth on an already oriented substrate[14] and the formation of oriented MOF crystallites on self-assembled monolayers (SAMs).[11,14,17] Generally, carboxyl-, hydroxyl-, or aza-heterocycle-terminated SAMs are used because of their capability to bind the metal nodes.[18–23] So far, vapor-phase MOF depositions either do not report orientation,[7,8,24] or when orientation was observed, the degree of orientation was not tunable while maintaining the optimized process parameters.[12,25–28]

Apart from deposition methods and control over crystallographic orientation, patterning MOF films will be critical for integration into electronics. Two MOF patterning approaches have been demonstrated: bottom-up and top-down. The bottom-up approach relies on the formation of the MOF material only in the desired areas, typically dictated by a patterned surface functionalization applied through stamping, microfluidics, or ink-jet printing.[29–36] The majority of studies following this approach combine liquid-phase epitaxy[17] with coordinating SAMs in the growth areas and non-coordinating SAMs (*e.g.*, $-CH_3$ or $-CF_3$) in the non-growth areas.[22,23,37] Similarly, non-coordinating SAMs are also employed to lower the adhesion of pre-formed MOF films in Langmuir-Blodgett depositions.[38,39] In the top-down approach, a thin film is initially deposited,

and specific sections are selectively removed via e-beam, UV or X-ray irradiation, followed by a development step.[29,40–42]

This study expands the scope of the MLD vapor-phase deposition process for ZIF-8 to oriented and patterned films. In our previous work on MLD of ZIF-8, a precursor layer with the same composition as the final MOF is first deposited through consecutive self-saturating surface reactions of diethyl zinc (DEZ), water, and 2-methylimidazole (HmIM). Subsequently, a linker exposure step promotes crystallization. The process parameters remain unaltered within this work to allow comparison between different surface terminations. We found that by using SAMs with different end groups, we could control the crystallographic orientation of ZIF-8 films from the vapor phase for the first time. In addition, since the mobility of the ZIF-8 building blocks during MLD depends on the surface functionalization, bottom-up MOF patterning dictated by an underlying SAM pattern could be realized.

Preferential crystallographic orientation

To investigate the effect of surface chemistry on ZIF-8 MLD, gold substrates were functionalized with thiol SAMs with three classes of end groups (**Figure 1**): non-coordinating (alkyl and phenyl), O-containing (alcohol and carboxyl), and N-containing (primary amine and imidazole). The choice of SAM precursors was guided by their chemical diversity and commercial availability. The quality of the grafted SAMs was verified by water contact angle measurements, a commonly used technique due to its accessibility and high-throughput nature (**Table S1, Figure S1**). ZIF-8 layers were deposited on top of these functionalized substrates via MLD, as reported before.[6] The degree of crystallographic orientation of the resulting films was evaluated via synchrotron grazing-incidence X-ray diffraction (GIXRD) measurements. Reciprocal space maps

(RSMs) provide a qualitative indication of crystallographic orientation as a radially non-uniform diffraction intensity for a particular Bragg reflection. The fraction of crystalline material that is preferentially oriented can be quantified through radial intensity distributions (RID), in which the intensity of the Bragg reflections at a specific Q-value are integrated and plotted as a function of the polar angle Chi (**Figure S2a**). After subtracting the background, the area within the 011 and 110 peaks indicates the fraction of oriented crystalline material. While the part of the signal that does not depend on Chi corresponds to the randomly oriented crystalline fraction (**Figure S2b**).[43]

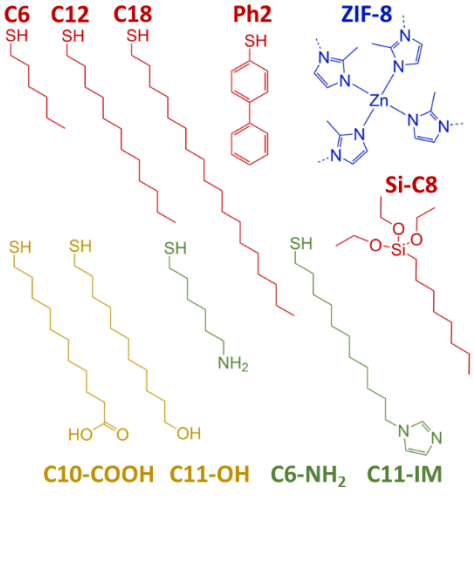

Figure 1. Molecules for SAM formation and the chemical structure of ZIF-8. C6, hexane thiol; C12, dodecane thiol; C18, octadodecane thiol; Ph2, biphenyl-4-thiol; ZIF-8, zeolitic imidazolate framework 8, zinc nodes connected by 2-methyl imidazole molecules; Si-C8, triethoxy(octyl)silane; C10-COOH, 11-mercaptoundecanoic acid; C11-OH, 11-mercaptoundecanol; C6-NH_2, 6-amino-1-hexane thiol; C11-IM, 1-(11-mercaptoundecyl)imidazole. Red for molecules with an alkyl or phenyl chain, green for nitrogen-containing molecules (*i.e.*, terminated with a primary amine or imidazole), and yellow for oxygen-containing molecules (*i.e.*, terminated with a hydroxyl or carboxylic acid group).

The RSM (**Figure 2b, S3)** and RIDs of the 011 reflection (**Figure 2c, S4**) show notable differences in the ZIF-8 film uniplanar texture depending on the SAM type. Perhaps surprisingly, the non-coordinating SAMs (alkyl and phenyl) result in the highest degree of crystallographic orientation (**Figure 2c-d**). Li *et al.* studied the solution deposition of ZIF-8 on non-coordinating alkyl SAMs and observed oriented MOF films as well, which they attributed to lattice matching between ZIF-8 and the SAM.[32] Lattice parameters can be defined for SAMs because of their highly regular packing, as previously evidenced by scanning tunneling microscopy, low-energy electron diffraction, and synchrotron GIXRD.[44–46] When the lattice parameters of the SAMs were altered by the presence of different end groups, solvent molecules adsorbed in the SAM, or changes in the metal layer, the oriented growth was disrupted. In our study, ZIF-8 MLD on the SAMs with alkyl chains (C6, C12, C18) resulted in highly oriented films (ca. 90% oriented, **Figure 2d, Table S2**), while the Ph2 SAM resulted in a slightly lower degree of crystallographic orientation (76 %), likely because of less ideal packing of the SAM, which is also indicated by a lower water contact angle (**Table S1**). Well-packed alkyl SAMs seem crucial for oriented growth since non-idealities will disrupt the lattice matching. ZIF-8 films deposited on the O-containing SAMs show an intermediate degree of crystallographic orientation, comparable to MLD deposition on a Si wafer with only a native SiO_2 layer (**Figure 2d**) or ZIF-8 CVD after extended linker exposure.[47] The N-containing SAMs resulted in randomly oriented ZIF-8 films (**Figure 2c-d**).

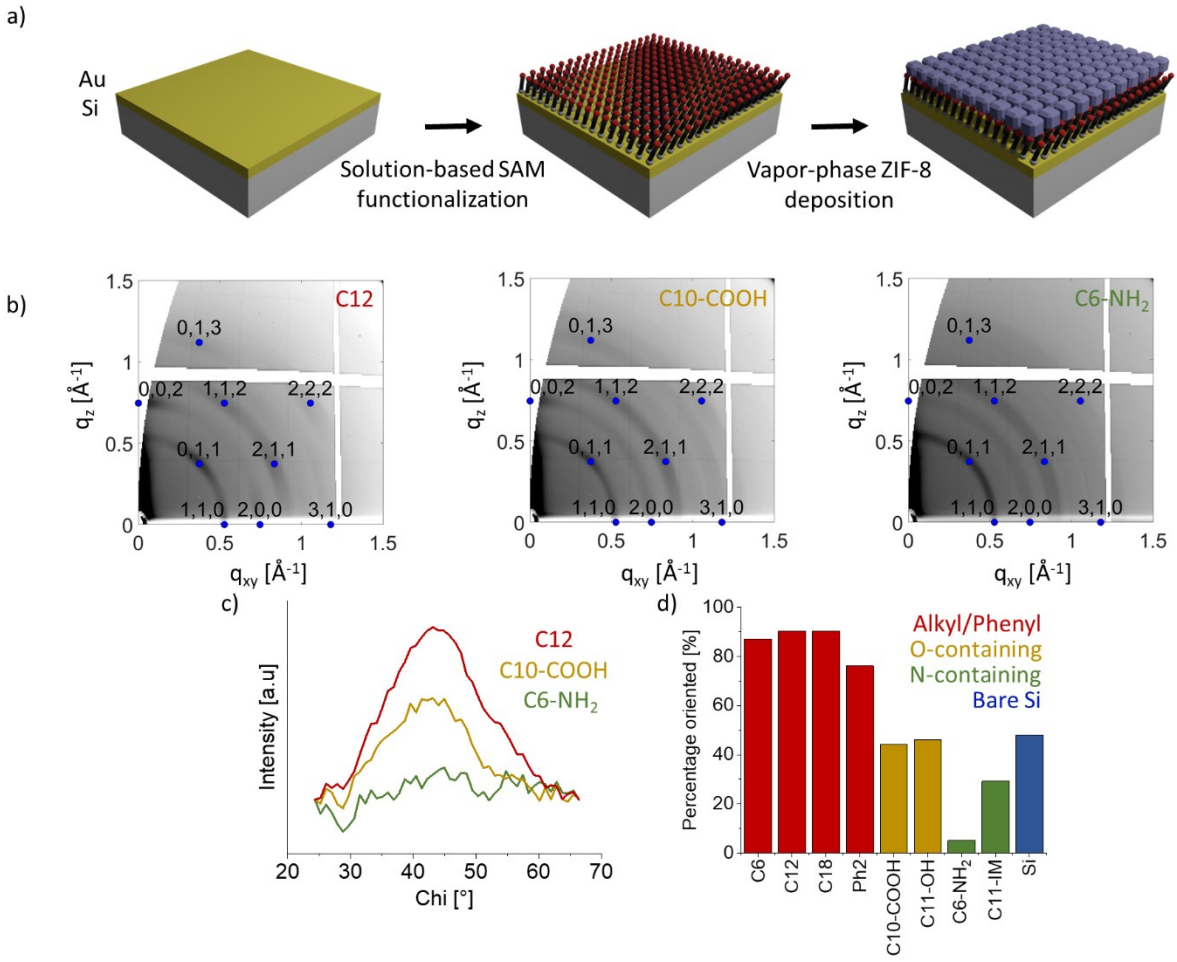

Figure 2. Preferential crystallographic orientation in ZIF-8 MLD films determined from synchrotron GIXRD measurements. a) Schematic representation of the sample preparation, b) RSMs of C12, C10-COOH and C6-NH_2. Labeled blue dots indicate simulated positions of Bragg peaks for a [001] orientation of ZIF-8 (VELVOY[48]). c) RID: intensities of the 011 reflections from the RSMs in panel (b) as a function of the Chi angle, with background and random contribution removed, d) Percentage crystalline material that is oriented for each tested SAM, percentage oriented = (oriented area/total area)·100. This calculation considers both the 011 and the 110 reflections.

Since the variations in crystallographic orientation are likely related to the interaction of the ZIF-8 building blocks with the functionalized substrate, an experiment was designed to probe the affinity of the linker for the different SAMs. The SAM-coated substrates were exposed to vaporized HmIM in the MLD reactor while being monitored with in-situ ellipsometry (**Figure 3a**). Ellipsometry is an optical film characterization technique that relies on the change in the amplitude (ψ) and phase (Δ) of s- and p-polarized light when reflected on a surface.[49] This technique is extremely sensitive to optical alterations of a film; for example, we previously utilized in-situ ellipsometry for monitoring individual MLD cycles.[6] The optical parameter Δ decreases with the amount of HmIM adsorbed since it is related to the optical film thickness. Carboxylic acid- and amine-terminated SAMs showed significant HmIM adsorption during dosing, though the molecules desorbed during the purge step (**Figure 3b**). In contrast, for the alkyl SAMs, HmIM adsorption was below the detection limit (**Figure 3b**, **S5a**), meaning that < 1 $\mu g/cm^2$ is present on the surface. These experiments indicate that HmIM adsorption alone does not explain the occurrence of oriented ZIF-8 growth.

Since we suspected intercalation of a small amount of HmIM into the alkyl SAMs, not directly detectable by ellipsometry, an indirect, amplification-based method was designed to probe the presence of adsorbed species. Similar to how the chemical amplification of a fluorescent signal in bio-assays enables the detection of trace quantities of analyte, atomic layer deposition (ALD) was used to detect the presence of HmIM in the alkyl SAMs. ALD is a thin film deposition technique based on consecutive self-saturating pulses of vaporized precursors that react with nucleation sites on the substrate. For ZnO ALD, the substrate is alternatingly exposed to DEZ and water vapor.[50,51] Since alkyl SAMs do not have reactive groups on which ZnO ALD can nucleate, many ALD cycles are needed before any ZnO is deposited. In other words, alkyl-terminated SAMs cause a nucleation

delay: >100 ALD cycles are required to grow 5 nm of ZnO on top of these SAMs, whereas only 35 cycles are needed on a bare wafer.[52] Since HmIM molecules intercalated into the alkyl-terminated SAMs could serve as nucleation sites, their presence would be observed as a reduction of the nucleation delay (**Figure 3c**). In addition, the reversible nature of the interaction between the intercalated HmIM molecules and the SAM could be demonstrated by varying the purge time between HmIM dosing and ZnO ALD. When purging for a longer time, hence removing more intercalated HmIM, the nucleation delay gradually approached that of the initial HmIM-free SAM (**Figure 3c**).

Based on these observations, we hypothesize that few HmIM molecules intercalate into the highly ordered alkyl SAM, without disturbing its regular nature. The presence of these oriented HmIM molecules on the surface likely explains the oriented ZIF-8 growth. Prior studies demonstrate that vapor-deposited benzene and pentacene films adopt the orientation of an underlying SAM through an intercalation mechanism, resulting in oriented growth.[53,54] To illustrate that intercalation is required for oriented ZIF-8 MLD films, and mere hydrophobicity is insufficient, the deposition was tested on a Si substrate coated with Hyflon, a perfluoroalkoxy polymer (**Figure S6a**), which forms a porous,[55,56] highly hydrophobic surface (water contact angle = 115.2°). As shown in **Figure S6**, no ZIF-8 was deposited on Hyflon. In this layer (~11 nm), HmIM can adsorb within the pores, but desorption occurs during the purge step because of the weak Van der Waals interactions (**Figure S5**).

The unique nature of the MLD approach becomes clear when compared with the earlier reported ZIF-8 CVD protocol (adapted from Tietze *et al.*[9]). In the CVD approach, a ZnO precursor layer deposited by ALD is progressively converted to ZIF-8 from the top down by exposing it to vaporized HmIM. However, when performed on the same SAM-functionalized surfaces, CVD

results in randomly oriented ZIF-8 films, even when ZnO precursor layers as thin as 1.5 nm are used (**Figure S7-8**), since the exposed surface during ZIF-8 formation is hydroxyl-terminated ZnO and not the underlying SAM. Therefore, the SAM cannot influence the crystallographic orientation of the ZIF-8 layer. In the case of MLD, the precursor layer with the same composition as ZIF-8 crystallizes in one step since no progressive linker penetration is needed as in CVD.

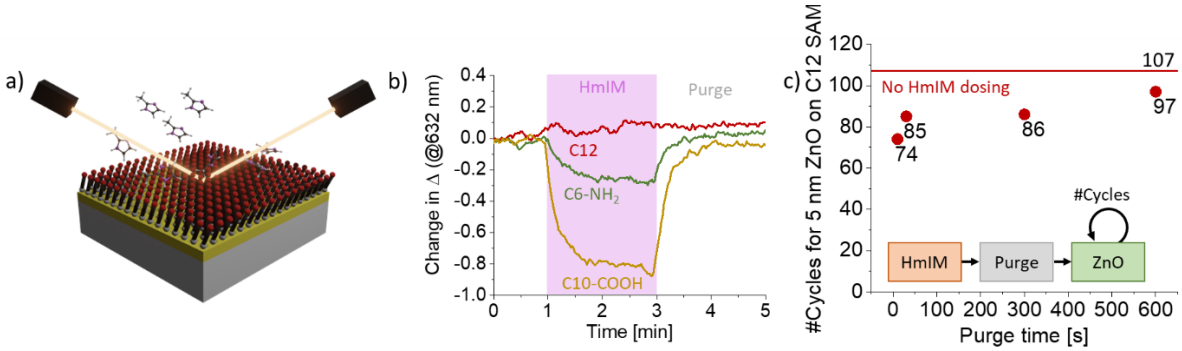

Figure 3. HmIM adsorption on SAM-functionalized surfaces. a) Schematic representation of an in-situ ellipsometry measurement of HmIM adsorption on a SAM-coated substrate. b) HmIM adsorption on C12, C6-NH_2, and C10-COOH SAMs monitored by in-situ ellipsometry and represented via a 10-point moving average of the change in Δ at 632 nm. c) Number of ALD cycles (DEZ + H_2O) needed to deposit 5 nm of ZnO ALD on C12 SAM (Y-axis). The purge time between HmIM dosing and the start of the ALD deposition is varied and is represented on the X-axis. Change in ZnO thickness was monitored by in-situ ellipsometry.

Precursor mobility and area-selective deposition

Our previous work reported rough ZIF-8 films with an incomplete coverage for two-step MLD on Si wafers with a native SiO_2 layer (RMS roughness 9.8 nm, **Figure S9**).[6] In that study, we observed surface mobility of the ZIF-8 building blocks during HmIM exposure resulting in Ostwald ripening.[6] In contrast, AFM images show that the ZIF-8 MLD precursor mobility on

alkyl- and phenyl-terminated and N-containing SAMs is strongly reduced relative to a native SiO_2 surface, resulting in smooth and continuous films (**Figure 4a, S9**). The hydroxyl-terminated SAM resulted in coverage similar to the bare wafer (C11-OH, **Figure S9**). On the other hand, a strong increase in precursor mobility is observed for a carboxylate SAM, leading to large, isolated crystallites (C10-COOH, **Figure 4a**). Surface mobility, rather than nucleation differences, primarily governs the variations in surface coverage. While the surface coverage achieved with C12, C10-COOH, and C6-NH_2 is ca. 96%, 50%, and 98%, respectively. In all cases, the total volume of MOF deposited, calculated from a 6 x 6 μm^2 area using flooding analysis on AFM data, is around 4.2×10^8 nm^3.

We hypothesized that these differences in mobility could be exploited to enable area-dependent surface diffusion,[57] and result in area-selective MLD of ZIF-8. Cu/SiO_2 patterns, as a model for Cu interconnects, were utilized to showcase this concept. These test patterns underwent chemical mechanical planarization to provide a planar top surface and exclude geometry effects (*e.g.*, because of raised copper lines). The copper lines were selectively functionalized with C10-COOH, since alkane thiols bind to copper as they do to gold.[58] Afterward, the remaining oxide surface was orthogonally functionalized with Si-C8 (triethoxy(octyl)silane), resulting in the hydrophobization of the SiO_2 regions (**Table S1**). The samples were only exposed to the precursor solution for a short time (4 h) to avoid Si-C8 deposition on the copper.[59] Finally, ZIF-8 was deposited via two-step MLD on this sample (**Figure 4b**). SEM-EDX and optical profilometry show that the building blocks move away from the copper lines due to the increased mobility of ZIF-8 precursors on C10-COOH (**Figure 4c-d, S10**). The reduced mobility on alkyl SAMs (Si-C8) is utilized to maximize the surface coverage between the Cu lines. Even without Si-C8 backfilling, area-selective

deposition is still achieved, utilizing the surface mobility observed on SiO_2 surfaces, though the ZIF-8 coverage in these areas is reduced (**Figure S11, S12**).

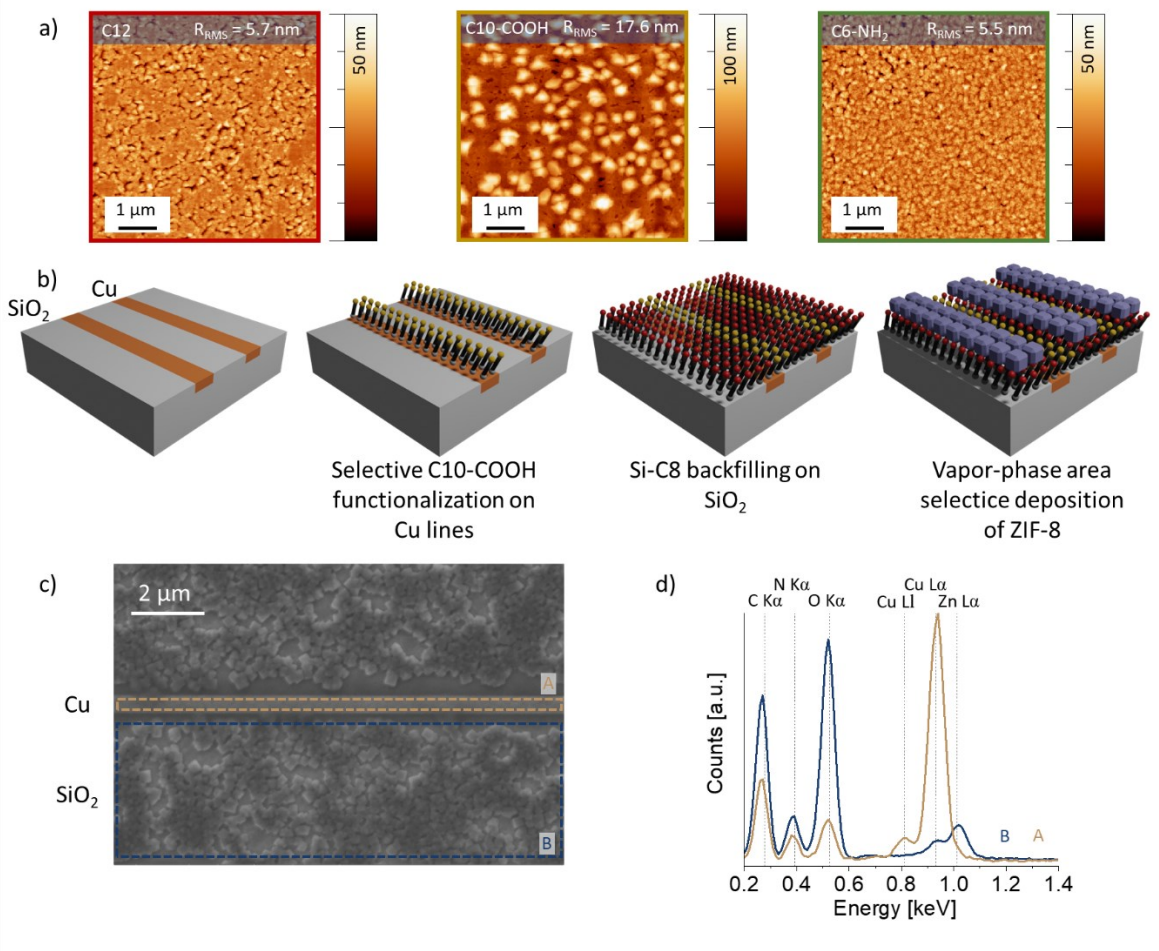

Figure 4. Mobility of ZIF-8 from MLD on SAM-functionalized surfaces. a) AFM topography images of ZIF-8 MLD on different SAMs (C12 left, C10-COOH middle, C6-NH_2 right). b) Schematic representation of the experimental approach used for vapor-phase area selective deposition of ZIF-8 on Cu/SiO_2 patterned substrates. c) SEM image of a ZIF-8 layer deposited on a Cu/SiO_2 pattern as described in panel (b). d) Selective area EDX spectra of the areas indicated on panel (c).

Conclusion

We demonstrated that SAM-functionalized substrates for ZIF-8 MLD enable both crystallographic orientation control and area-selective deposition of the MOF films. Alkyl and phenyl SAMs result in the highest degree of preferential orientation, while N-containing SAMs lead to randomly oriented ZIF-8. O-containing SAMs, on the other hand, yield intermediate results. We hypothesize that small amounts of HmIM intercalate into the alkyl and phenyl SAMs, without disturbing the regular packing and lattice matching, to provide nucleation sites for oriented growth. Additionally, alkyl, phenyl and N-containing SAMs can be used to achieve high ZIF-8 film coverages with low roughness, whereas carboxylic acid SAMs result in a high mobility of the building blocks on the surface. These differences in surface mobility could be exploited to realize area-selective ZIF-8 MLD.

ASSOCIATED CONTENT

The Supporting Information is available free of charge on the ACS Publications website: methods section; water contact angle measurements of all used surfaces; illustration of synchrotron GIXRD data processing; RSMs; RIDs; table containing calculated oriented area, total area, and percentage oriented of all SAMs; HmIM adsorption experiments; Hyflon substrate depositions; ZIF-8 CVD on SAM functionalized surfaces; ZIF-8 CVD on SAM functionalized surfaces with decreasing ZnO precursor thickness; AFM illustrating mobility; optical profilometry of C10-COOH and Si-C8 functionalized Cu/SiO_2 patterns; SEM-EDX of C10-COOH functionalized Cu/SiO_2 pattern without Si-C8 backfilling; optical profilometry of C10-COOH functionalized Cu/SiO_2 patterns without Si-C8 backfilling.

AUTHOR INFORMATION

Corresponding Author

* E-mail: rob.ameloot@kuleuven.be

Present Addresses

† Instituto de Ciencia Molecular (ICMol), Universitat de València, Catedrático José Beltrán 2, 46980 Paterna, Spain

§ Department of Physics, Aberystwyth University, SY23 3BZ Aberystwyth, United Kingdom

Author Contributions

The manuscript was written through contributions of all authors. All authors have given approval to the final version of the manuscript.

ACKNOWLEDGMENT

This project has received funding from the European Research Council (ERC) under the European Union's Horizon 2020 research and innovation program (grant agreement n° 716472, acronym VAPORE), from the Research Foundation Flanders (FWO Vlaanderen) in projects G085720N and G087422N, from VLAIO in project moonshot project TEMPEL HBC.2021.0580, and from KU Leuven in project C14/20/085. J.S., V.R.-G., J.G.-L., and J.A. acknowledge the support of the FWO Vlaanderen for their respective fellowships 11H8123N, 1263622N, 12E5123N, and 1S89724N. R.R. and S.D.F. acknowledge funding from the FWO (G0H2122N) and F.R.S.-FNRS under the Excellence of Science (EOS 40007495) program. This project has received funding from the European Union's Horizon 2020 Research and Innovation Program under the Marie Sklodowska-Curie grant agreement No. 888163. R.N. acknowledges financial support by the European Research Council (ERC CoG No. 815128 REALNANO). We acknowledge Prof. Sara Bals for providing access to electron microscopy facilities. The authors

want to thank Mikhail Krishtab and Giel Arnauts for fruitful discussions. We acknowledge Elettra Syncrotrone Trieste for providing access to its synchrotron radiation facilities (proposal n° 20210060, and 20220410) and thank Luisa Barba and Giorgio Bais for assistance in using beamline XRD1. We acknowledge Diamond Light Source for time on Beamline I07 under Proposal SI31693 and SI33460 and thank Francesco Carlà and Jonathan Rawle. We acknowledge ESRF synchrotron for beamtime on DUBBLE BM26 and thank Martin Rosenthal for assistance and support. The research leading to this result has been supported by the project CALIPSOplus under Grant Agreement 730872 from the EU Framework Programme for Research and Innovation HORIZON 2020.

ABBREVIATIONS

MOF, metal-organic framework; ZIF-8, zeolitic imidazolate framework-8; MLD, molecular layer deposition; CVD, chemical vapor deposition; SAM, self-assembled monolayer; DEZ, diethyl zinc; HmIM, 2-methyl imidazole; GIXRD, Grazing incidence X-ray diffraction; AFM, atomic force microscopy; RSM, reciprocal space map; RID, radial intensity distribution; ALD, atomic layer deposition; SEM-EDX, Scanning electron microscopy with energy dispersive X-ray.

REFERENCES

(1) Aizenberg, J.; Black, A. J.; Whitesides, G. M. Control of Crystal Nucleation by Patterned Self-Assembled Monolayers. *Nature* **1999**, *398* (6727), 495–498. https://doi.org/10.1038/19047.

(2) Krishtab, M.; Stassen, I.; Stassin, T.; Cruz, A. J.; Okudur, O. O.; Armini, S.; Wilson, C.; De Gendt, S.; Ameloot, R. Vapor-Deposited Zeolitic Imidazolate Frameworks as Gap-Filling Ultra-Low-k Dielectrics. *Nat. Commun.* **2019**, *10* (1), 3729. https://doi.org/10.1038/s41467-019-11703-x.

(3) Stassen, I.; Burtch, N.; Talin, A.; Falcaro, P.; Allendorf, M.; Ameloot, R. An Updated Roadmap for the Integration of Metal–Organic Frameworks with Electronic Devices and Chemical Sensors. *Chem. Soc. Rev.* **2017**, *46* (11), 3185–3241. https://doi.org/10.1039/C7CS00122C.

(4) Usman, M.; Mendiratta, S.; Lu, K.-L. Semiconductor Metal–Organic Frameworks: Future Low-Bandgap Materials. *Adv. Mater.* **2017**, *29* (6), 1605071. https://doi.org/10.1002/adma.201605071.
(5) Su, P.; Tu, M.; Ameloot, R.; Li, W. Vapor-Phase Processing of Metal–Organic Frameworks. *Acc. Chem. Res.* **2022**, *55* (2), 186–196. https://doi.org/10.1021/acs.accounts.1c00600.
(6) Smets, J.; Cruz, A. J.; Rubio-Giménez, V.; Tietze, M. L.; Kravchenko, D. E.; Arnauts, G.; Matavž, A.; Wauteraerts, N.; Tu, M.; Marcoen, K.; Imaz, I.; Maspoch, D.; Korytov, M.; Vereecken, P. M.; De Feyter, S.; Hauffman, T.; Ameloot, R. Molecular Layer Deposition of Zeolitic Imidazolate Framework-8 Films. *Chem. Mater.* **2023**, *35* (4), 1684–1690. https://doi.org/10.1021/acs.chemmater.2c03439.
(7) Cruz, A. J.; Stassen, I.; Krishtab, M.; Marcoen, K.; Stassin, T.; Rodríguez-Hermida, S.; Teyssandier, J.; Pletincx, S.; Verbeke, R.; Rubio-Giménez, V.; Tatay, S.; Martí-Gastaldo, C.; Meersschaut, J.; Vereecken, P. M.; De Feyter, S.; Hauffman, T.; Ameloot, R. Integrated Cleanroom Process for the Vapor-Phase Deposition of Large-Area Zeolitic Imidazolate Framework Thin Films. *Chem. Mater.* **2019**, *31* (22), 9462–9471. https://doi.org/10.1021/acs.chemmater.9b03435.
(8) Stassen, I.; Styles, M.; Grenci, G.; Gorp, H. V.; Vanderlinden, W.; Feyter, S. D.; Falcaro, P.; Vos, D. D.; Vereecken, P.; Ameloot, R. Chemical Vapour Deposition of Zeolitic Imidazolate Framework Thin Films. *Nat. Mater.* **2016**, *15* (3), 304–310. https://doi.org/10.1038/nmat4509.
(9) Tietze, M. L.; Obst, M.; Arnauts, G.; Wauteraerts, N.; Rodríguez-Hermida, S.; Ameloot, R. Parts-per-Million Detection of Volatile Organic Compounds via Surface Plasmon Polaritons and Nanometer-Thick Metal–Organic Framework Films. *ACS Appl. Nano Mater.* **2022**, acsanm.2c00012. https://doi.org/10.1021/acsanm.2c00012.
(10) Fu, Z.; Xu, G. Crystalline, Highly Oriented MOF Thin Film: The Fabrication and Application. *Chem. Rec.* **2017**, *17* (5), 518–534. https://doi.org/10.1002/tcr.201600109.
(11) Khalil, I. E.; Fonseca, J.; Reithofer, M. R.; Eder, T.; Chin, J. M. Tackling Orientation of Metal-Organic Frameworks (MOFs): The Quest to Enhance MOF Performance. *Coord. Chem. Rev.* **2023**, *481*, 215043. https://doi.org/10.1016/j.ccr.2023.215043.
(12) Rubio-Giménez, V.; Arnauts, G.; Wang, M.; Oliveros Mata, E. S.; Huang, X.; Lan, T.; Tietze, M. L.; Kravchenko, D. E.; Smets, J.; Wauteraerts, N.; Khadiev, A.; Novikov, D. V.; Makarov, D.; Dong, R.; Ameloot, R. Chemical Vapor Deposition and High-Resolution Patterning of a Highly Conductive Two-Dimensional Coordination Polymer Film. *J. Am. Chem. Soc.* **2023**, *145* (1), 152–159. https://doi.org/10.1021/jacs.2c09007.
(13) Contreras-Pereda, N.; Rodríguez-San-Miguel, D.; Franco, C.; Sevim, S.; Vale, J. P.; Solano, E.; Fong, W.-K.; Del Giudice, A.; Galantini, L.; Pfattner, R.; Pané, S.; Mayor, T. S.; Ruiz-Molina, D.; Puigmartí-Luis, J. Synthesis of 2D Porous Crystalline Materials in Simulated Microgravity. *Adv. Mater.* **2021**, *33* (30), 2101777. https://doi.org/10.1002/adma.202101777.
(14) Linares-Moreau, M.; Brandner, L. A.; Velásquez-Hernández, M. de J.; Fonseca, J.; Benseghir, Y.; Chin, J. M.; Maspoch, D.; Doonan, C.; Falcaro, P. Fabrication of Oriented Polycrystalline MOF Superstructures. *Adv. Mater.* **2024**, *36* (1), 2309645. https://doi.org/10.1002/adma.202309645.
(15) Hong, T.; Lee, C.; Bak, Y.; Park, G.; Lee, H.; Kang, S.; Bae, T.-H.; Yoon, D. K.; Park, J. G. On-Demand Tunable Electrical Conductance Anisotropy in a MOF-Polymer Composite. *Small* **2024**, *20* (18), 2309469. https://doi.org/10.1002/smll.202309469.

(16) Ha, D.-G.; Rezaee, M.; Han, Y.; Siddiqui, S. A.; Day, R. W.; Xie, L. S.; Modtland, B. J.; Muller, D. A.; Kong, J.; Kim, P.; Dincă, M.; Baldo, M. A. Large Single Crystals of Two-Dimensional π-Conjugated Metal–Organic Frameworks via Biphasic Solution-Solid Growth. *ACS Cent. Sci.* **2021**, *7* (1), 104–109. https://doi.org/10.1021/acscentsci.0c01488.
(17) Zhuang, J.-L.; Terfort, A.; Wöll, C. Formation of Oriented and Patterned Films of Metal–Organic Frameworks by Liquid Phase Epitaxy: A Review. *Coord. Chem. Rev.* **2016**, *307*, 391–424. https://doi.org/10.1016/j.ccr.2015.09.013.
(18) Shekhah, O.; Wang, H.; Zacher, D.; Fischer, R. A.; Wöll, C. Growth Mechanism of Metal–Organic Frameworks: Insights into the Nucleation by Employing a Step-by-Step Route. *Angew. Chem. Int. Ed.* **2009**, *48* (27), 5038–5041. https://doi.org/10.1002/anie.200900378.
(19) Zacher, D.; Yusenko, K.; Bétard, A.; Henke, S.; Molon, M.; Ladnorg, T.; Shekhah, O.; Schüpbach, B.; de los Arcos, T.; Krasnopolski, M.; Meilikhov, M.; Winter, J.; Terfort, A.; Wöll, C.; Fischer, R. A. Liquid-Phase Epitaxy of Multicomponent Layer-Based Porous Coordination Polymer Thin Films of [M(L)(P)0.5] Type: Importance of Deposition Sequence on the Oriented Growth. *Chem. – Eur. J.* **2011**, *17* (5), 1448–1455. https://doi.org/10.1002/chem.201002381.
(20) Scherb, C.; Schödel, A.; Bein, T. Directing the Structure of Metal–Organic Frameworks by Oriented Surface Growth on an Organic Monolayer. *Angew. Chem. Int. Ed.* **2008**, *47* (31), 5777–5779. https://doi.org/10.1002/anie.200704034.
(21) Wannapaiboon, S.; Schneemann, A.; Hante, I.; Tu, M.; Epp, K.; Semrau, A. L.; Sternemann, C.; Paulus, M.; Baxter, S. J.; Kieslich, G.; Fischer, R. A. Control of Structural Flexibility of Layered-Pillared Metal-Organic Frameworks Anchored at Surfaces. *Nat. Commun.* **2019**, *10* (1), 346. https://doi.org/10.1038/s41467-018-08285-5.
(22) Shekhah, O.; Wang, H.; Kowarik, S.; Schreiber, F.; Paulus, M.; Tolan, M.; Sternemann, C.; Evers, F.; Zacher, D.; Fischer, R. A.; Wöll, C. Step-by-Step Route for the Synthesis of Metal−Organic Frameworks. *J. Am. Chem. Soc.* **2007**, *129* (49), 15118–15119. https://doi.org/10.1021/ja076210u.
(23) Biemmi, E.; Scherb, C.; Bein, T. Oriented Growth of the Metal Organic Framework Cu3(BTC)2(H2O)3·xH2O Tunable with Functionalized Self-Assembled Monolayers. *J. Am. Chem. Soc.* **2007**, *129* (26), 8054–8055. https://doi.org/10.1021/ja0701208.
(24) Tu, M.; Kravchenko, D. E.; Xia, B.; Rubio-Giménez, V.; Wauteraerts, N.; Verbeke, R.; Vankelecom, I. F. J.; Stassin, T.; Egger, W.; Dickmann, M.; Amenitsch, H.; Ameloot, R. Template-Mediated Control over Polymorphism in the Vapor-Assisted Formation of Zeolitic Imidazolate Framework Powders and Films. *Angew. Chem. Int. Ed.* **2021**, *60* (14), 7553–7558. https://doi.org/10.1002/anie.202014791.
(25) Rodríguez-Hermida, S.; Kravchenko, D. E.; Wauteraerts, N.; Ameloot, R. Vapor-Assisted Powder Synthesis and Oriented MOF-CVD Thin Films of the Metal–Organic Framework HKUST-1. *Inorg. Chem.* **2022**, *61* (45), 17927–17931. https://doi.org/10.1021/acs.inorgchem.2c02490.
(26) Choe, M.; Koo, J. Y.; Park, I.; Ohtsu, H.; Shim, J. H.; Choi, H. C.; Park, S. S. Chemical Vapor Deposition of Edge-on Oriented 2D Conductive Metal–Organic Framework Thin Films. *J. Am. Chem. Soc.* **2022**, *144* (37), 16726–16731. https://doi.org/10.1021/jacs.2c07135.
(27) Stassin, T.; Rodríguez-Hermida, S.; Schrode, B.; Cruz, A. J.; Carraro, F.; Kravchenko, D.; Creemers, V.; Stassen, I.; Hauffman, T.; Vos, D. D.; Falcaro, P.; Resel, R.; Ameloot, R. Vapour-Phase Deposition of Oriented Copper Dicarboxylate Metal–Organic Framework

Thin Films. *Chem. Commun.* **2019**, *55* (68), 10056–10059. https://doi.org/10.1039/C9CC05161A.
(28) Legenstein, L.; Rodríguez-Hermida, S.; Rubio-Giménez, V.; Stassin, T.; Hofer, S.; Kainz, M. P.; Fratschko, M.; Carraro, F.; Falcaro, P.; Ameloot, R.; Resel, R. Identifying the Internal Network Structure of a New Copper Isonicotinate Thin-Film Polymorph Obtained via Chemical Vapor Deposition. *Adv. Mater. Interfaces* **2023**, *10* (12), 2202461. https://doi.org/10.1002/admi.202202461.
(29) Falcaro, P.; Ricco, R.; Doherty, C. M.; Liang, K.; Hill, A. J.; Styles, M. J. MOF Positioning Technology and Device Fabrication. *Chem. Soc. Rev.* **2014**, *43* (16), 5513–5560. https://doi.org/10.1039/C4CS00089G.
(30) Ruiz-Zambrana, C. L.; Malankowska, M.; Coronas, J. Metal Organic Framework Top-down and Bottom-up Patterning Techniques. *Dalton Trans.* **2020**, *49* (43), 15139–15148. https://doi.org/10.1039/D0DT02207A.
(31) Falcaro, P.; Buso, D.; Hill, A. J.; Doherty, C. M. Patterning Techniques for Metal Organic Frameworks. *Adv. Mater.* **2012**, *24* (24), 3153–3168. https://doi.org/10.1002/adma.201200485.
(32) Li, S.; Shi, W.; Lu, G.; Li, S.; Loo, S. C. J.; Huo, F. Unconventional Nucleation and Oriented Growth of ZIF-8 Crystals on Non-Polar Surface. *Adv. Mater.* **2012**, *24* (44), 5954–5958. https://doi.org/10.1002/adma.201201996.
(33) Miao, Y.; Lee, D. T.; de Mello, M. D.; Ahmad, M.; Abdel-Rahman, M. K.; Eckhert, P. M.; Boscoboinik, J. A.; Fairbrother, D. H.; Tsapatsis, M. Solvent-Free Bottom-up Patterning of Zeolitic Imidazolate Frameworks. *Nat. Commun.* **2022**, *13* (1), 420. https://doi.org/10.1038/s41467-022-28050-z.
(34) Kravchenko, D. E.; Matavž, A.; Rubio-Giménez, V.; Vanduffel, H.; Verstreken, M.; Ameloot, R. Aerosol Jet Printing of the Ultramicroporous Calcium Squarate Metal–Organic Framework. *Chem. Mater.* **2022**, *34* (15), 6809–6814. https://doi.org/10.1021/acs.chemmater.2c00947.
(35) Ameloot, R.; Gobechiya, E.; Uji-i, H.; Martens, J. A.; Hofkens, J.; Alaerts, L.; Sels, B. F.; De Vos, D. E. Direct Patterning of Oriented Metal–Organic Framework Crystals via Control over Crystallization Kinetics in Clear Precursor Solutions. *Adv. Mater.* **2010**, *22* (24), 2685–2688. https://doi.org/10.1002/adma.200903867.
(36) Kar, P.; Wang, C.-M.; Liao, C.-L.; Chang, T.-S.; Liao, W.-S. Guiding Metal Organic Framework Morphology via Monolayer Artificial Defect-Induced Preferential Facet Selection. *JACS Au* **2023**, jacsau.2c00692. https://doi.org/10.1021/jacsau.2c00692.
(37) Hermes, S.; Schröder, F.; Chelmowski, R.; Wöll, C.; Fischer, R. A. Selective Nucleation and Growth of Metal−Organic Open Framework Thin Films on Patterned COOH/CF3-Terminated Self-Assembled Monolayers on Au(111). *J. Am. Chem. Soc.* **2005**, *127* (40), 13744–13745. https://doi.org/10.1021/ja053523l.
(38) Rubio-Giménez, V.; Galbiati, M.; Castells-Gil, J.; Almora-Barrios, N.; Navarro-Sánchez, J.; Escorcia-Ariza, G.; Mattera, M.; Arnold, T.; Rawle, J.; Tatay, S.; Coronado, E.; Martí-Gastaldo, C. Bottom-Up Fabrication of Semiconductive Metal–Organic Framework Ultrathin Films. *Adv. Mater.* **2018**, *30* (10), 1704291. https://doi.org/10.1002/adma.201704291.
(39) Rubio-Giménez, V.; Tatay, S.; Volatron, F.; Martínez-Casado, F. J.; Martí-Gastaldo, C.; Coronado, E. High-Quality Metal–Organic Framework Ultrathin Films for Electronically Active Interfaces. *J. Am. Chem. Soc.* **2016**, *138* (8), 2576–2584. https://doi.org/10.1021/jacs.5b09784.

(40) Tu, M.; Xia, B.; Kravchenko, D. E.; Tietze, M. L.; Cruz, A. J.; Stassen, I.; Hauffman, T.; Teyssandier, J.; De Feyter, S.; Wang, Z.; Fischer, R. A.; Marmiroli, B.; Amenitsch, H.; Torvisco, A.; Velásquez-Hernández, M. de J.; Falcaro, P.; Ameloot, R. Direct X-Ray and Electron-Beam Lithography of Halogenated Zeolitic Imidazolate Frameworks. *Nat. Mater.* **2020**, 1–7. https://doi.org/10.1038/s41563-020-00827-x.
(41) Miao, Y.; Tsapatsis, M. Electron Beam Patterning of Metal–Organic Frameworks. *Chem. Mater.* **2021**, *33* (2), 754–760. https://doi.org/10.1021/acs.chemmater.0c04204.
(42) Zhu, Z.; Li, F.; Li, J.; Chen, Q.; Li, W.; Tang, Z.; Xu, W.; Shen, W.; Tao, T. H.; Sun, L.; Fu, Y.; Tu, M. Direct Optical Patterning of Metal–Organic Frameworks via Photoacid–Induced Etching. *ACS Nano* **2024**. https://doi.org/10.1021/acsnano.4c04213.
(43) Fischer, J. C.; Li, C.; Hamer, S.; Heinke, L.; Herges, R.; Richards, B. S.; Howard, I. A. GIWAXS Characterization of Metal–Organic Framework Thin Films and Heterostructures: Quantifying Structure and Orientation. *Adv. Mater. Interfaces* **2023**, *10* (11), 2202259. https://doi.org/10.1002/admi.202202259.
(44) Liu, J.; Schüpbach, B.; Bashir, A.; Shekhah, O.; Nefedov, A.; Kind, M.; Terfort, A.; Wöll, C. Structural Characterization of Self-Assembled Monolayers of Pyridine-Terminated Thiolates on Gold. *Phys. Chem. Chem. Phys.* **2010**, *12* (17), 4459. https://doi.org/10.1039/b924246p.
(45) Fenter, P.; Eberhardt, A.; Eisenberger, P. Self-Assembly of n-Alkyl Thiols as Disulfides on Au(111). *Science* **1994**, *266* (5188), 1216–1218. https://doi.org/10.1126/science.266.5188.1216.
(46) Gerlach, R.; Polanski, G.; Rubahn, H.-G. Growth of Ultrathin Organic Films on Au(111) Surfaces. *Thin Solid Films* **1998**, *318* (1), 270–272. https://doi.org/10.1016/S0040-6090(97)01188-7.
(47) Kräuter, M.; Cruz, A. J.; Stassin, T.; Rodríguez-Hermida, S.; Ameloot, R.; Resel, R.; Coclite, A. M. Influence of Precursor Density and Conversion Time on the Orientation of Vapor-Deposited ZIF-8. *Crystals* **2022**, *12* (2), 217. https://doi.org/10.3390/cryst12020217.
(48) Park, K. S.; Ni, Z.; Cote, A. P.; Choi, J. Y.; Huang, R.; Uribe-Romo, F. J.; Chae, H. K.; O'Keeffe, M.; Yaghi, O. M. CCDC 602542: Experimental Crystal Structure Determination, 2006. https://doi.org/10.5517/CCN6ZVN.
(49) Tompkins, H. G.; Hilfiker, J. N. *Spectroscopic Ellipsometry: Practical Application to Thin Film Characterization*; Materials characterization and analysis collection; Momentum Press: New York, NY, 2016.
(50) Van Ommen, J. R.; Goulas, A.; Puurunen, R. L. Atomic Layer Deposition. In *Kirk-Othmer Encyclopedia of Chemical Technology*; Kirk-Othmer, Ed.; Wiley, 2021; pp 1–42. https://doi.org/10.1002/0471238961.koe00059.
(51) Weckman, T.; Laasonen, K. Atomic Layer Deposition of Zinc Oxide: Diethyl Zinc Reactions and Surface Saturation from First-Principles. *J. Phys. Chem. C* **2016**, *120* (38), 21460–21471. https://doi.org/10.1021/acs.jpcc.6b06141.
(52) Li, J.; Chai, G.; Wang, X. Atomic Layer Deposition of Thin Films: From a Chemistry Perspective. *Int. J. Extreme Manuf.* **2023**, *5* (3), 032003. https://doi.org/10.1088/2631-7990/acd88e.
(53) Hu, W. S.; Tao, Y. T.; Hsu, Y. J.; Wei, D. H.; Wu, Y. S. Molecular Orientation of Evaporated Pentacene Films on Gold: Alignment Effect of Self-Assembled Monolayer. *Langmuir* **2005**, *21* (6), 2260–2266. https://doi.org/10.1021/la047634u.

(54) Yuan, H.; Gibson, K. D.; Killelea, D. R.; Sibener, S. J. Alignment of Benzene Thin Films on Self-Assembled Monolayers by Surface Templating. *Surf. Sci.* **2013**, *609*, 177–182. https://doi.org/10.1016/j.susc.2012.12.005.
(55) Macchione, M.; Jansen, J. C.; De Luca, G.; Tocci, E.; Longeri, M.; Drioli, E. Experimental Analysis and Simulation of the Gas Transport in Dense Hyflon® AD60X Membranes: Influence of Residual Solvent. *Polymer* **2007**, *48* (9), 2619–2635. https://doi.org/10.1016/j.polymer.2007.02.068.
(56) Arcella, V.; Colaianna, P.; Maccone, P.; Sanguineti, A.; Gordano, A.; Clarizia, G.; Drioli, E. A Study on a Perfluoropolymer Purification and Its Application to Membrane Formation. *J. Membr. Sci.* **1999**, *163* (2), 203–209. https://doi.org/10.1016/S0376-7388(99)00184-2.
(57) Grillo, F.; Soethoudt, J.; Marques, E. A.; de Martín, L.; Van Dongen, K.; van Ommen, J. R.; Delabie, A. Area-Selective Deposition of Ruthenium by Area-Dependent Surface Diffusion. *Chem. Mater.* **2020**, acs.chemmater.0c02588. https://doi.org/10.1021/acs.chemmater.0c02588.
(58) Telegdi, J. Formation of Self-Assembled Anticorrosion Films on Different Metals. *Materials* **2020**, *13* (22), 5089. https://doi.org/10.3390/ma13225089.
(59) Maestre Caro, A.; Zhao, L.; Maes, G.; Borghs, G.; Beyer, G.; Tokei, Z.; Armini, S.; Travaly, Y. High Quality NH2SAM (Self Assembled Monolayer) Diffusion Barrier for Advanced Copper Interconnects. *MRS Online Proc. Libr.* **2010**, *1249* (1), 201. https://doi.org/10.1557/PROC-1249-F02-01.

ToC graphic